Accurate interaction between silver(I) ion and amino acid side chains with the 12-6 Lennard-Jones potential: a bottom-up parameterization approach

Luca Manciocchi[a], Alexandre Bianchi[b], Valérie Mazan[c], Mark Potapov[a], Katharina Fromm[b], and Martin Spichty[a]

[a]Laboratoire d'Innovation Moléculaire et Applications (LIMA) – UMR 7042, 3 bis, rue Alfred Werner, 68093, Mulhouse, France.

[b]University of Fribourg, Department of Chemistry, Chemin du Musée 9, CH-1700 Fribourg, Switzerland.

[c]Laboratoire d'Innovation Moléculaire et Applications (LIMA) – UMR 7042, 25 rue Becquerel, 67000, Strasbourg, France.

Abstract

Silver(I) ions and organometallic complexes thereof are well established antimicrobic agents. They have been used in medical applications for many centuries. It is also known that some bacteria can resist to silver(I) treatments by means of an efflux mechanism guided by a set of silver-binding transport proteins (e.g., SilE/F) and transmembrane channel. The exact mechanism of action, however, is not fully clear yet. All-atom force-field simulations can provide valuable structural and thermodynamic insights on the molecular processes of the underlying mechanism. Lennard-Jones parameters of silver(I) have been available for quite some time; their applicability to describe properly the binding properties (affinity, binding distance) between silver(I) and peptide-based binding motifs remains, however, an open question. We show here that the standard 12-6 Lennard-Jones parameters (previously developed to describe the hydration free energy with the TIP3P water model) drastically underestimate the strength of interaction between silver(I) and methionine as well as histidine. These are two key residues of the silver(I)-binding motifs in the transport proteins SilE/F. Using free-energy calculations, we calibrated the 12-6 Lennard-Jones parameters for the CHARMM36m force field to reproduce the experimental binding constant between amino acid side chain fragments and silver(I) ions. We then successfully validated the new parameters on a set of small silver-binding peptides with experimentally known binding constants. In addition, we could monitor how silver(I) ions increase the α-helical content of the LP1 oligopeptide, in agreement with previously reported Circular Dichroism (CD) experiments. Future improvements are outlined. The integration of these new parameters is straightforward for most simulation packages. It sets the stage for the modeling community to study more complex silver(I)-binding processes such as with the transporter proteins SilE/F.

1 Introduction: scientific context

The antimicrobic properties of silver(I) ions are well known and applied in various medical solutions. However, some bacteria are known to resist to silver(I) cytotoxicity through an efflux pump mechanism which allows them to expel the ion from the cytoplasm.[1–5] The efflux occurs through the transmembrane ion channel CusCBA. In addition, silver(I)-binding transporter proteins, such as SilE and SilF, are involved that act as a sponge and take out silver(I) ions from the cytoplasm to transfer them to the CusCBA channel.

Particularly important for the binding of silver(I) ions to the protein-based sponges are the amino acids histidine (H) and methionine (M). The motifs HXXM and MXXH are privileged binding motifs for silver(I) ions.[6] The influence of the bridging residues XX on the affinity has been studied in great detail,[7] and some tendencies were identified. Their impact, however, on the dynamic structure of the peptide and the binding affinity is not fully understood yet.

An interesting observation is also that silver(I) binding to non-structured proteins and peptides induces the formation of structured, alpha-helical motifs. The actual molecular mechanism remains unclear.[6,8,9]

All-atom molecular dynamics simulations on the nano- to microsecond timescale could provide valuable insights into these open questions. Force-filed parameters for silver(I) ions haven been developed previously: Won parametrized monovalent ions including silver(I) to reproduce the hydration free energy (HFE) for Jorgensen's TIP3P water model. Unfortunately, these parameters were not correctly integrated into CHARMM force field (lacking the proper conversion from kilojoules to kilocalories), for example, when obtaining them from CHARMM-GUI server. Merz and coworkers determined alternative 12-6 LJ silver(I) parameters. They aimed to reproduce either the hydration free energy (HFE) or the ion-oxygen distance (IOD) for multiple water models.[10] A 12-6-4 LJ model was also proposed to account for polarizability. The Merz group later proposed specific 12-6-4 LJ parameters for the interaction of silver(I) (among other metal ions) with imidazole and acetate.[11,12] While the 12-6-4 LJ potential is certainly a valuable extension it is not available in most simulation packages by default. We therefore focus only on the standard 12-6 LJ potential.

In this work we first test if the above 12-6 LJ literature parameters can be directly applied to actually study the interaction of silver(I) ions with a HXXM binding motif described by the CHARMM36m force field. We then present the development of improved 12-6 LJ parameters for the interaction of silver(I) with histidine, methionine and toluene. We thereby employed a bottom up strategy: we first developed parameters for the silver(I) interaction with sidechain fragments for which affinity data was available from literature or that we measured by potentiometric or spectrophotometric titrations. We then validated the obtained parameters against binding constants data for HXXM and MXXH binding motifs measured from NMR titrations.[7] Finally, as an application of the new parameters, we tested them against structural data for the peptide LP1 (called B1b in [9]), in particular the transition from an intrinsically disordered peptide to an alpha-helical structure in the presence of silver(I) ions.

2 Methodology

This section provides a general outline of the chosen methodology. Details of the applied computational procedures are given in the Supplementary Information (ESI).

2.1 Preliminary evaluations

As an initial test, Won's parameters and Merz' HFE and IOD parameter sets were tested against a strong silver-binding tetrapeptide: HEFM.[6,10] As shown in the section "Results & Discussion", all three sets drastically underestimated the binding affinity of HEFM and silver(I) (Table 1).

An intuitive strategy to analyze and eventually correct the underestimated affinity is to adopt a bottom-up approach by studying the interaction of each amino acid sidechain fragment with silver(I).[13] For example, 4-ethylimidazol was chosen as analogue for the histidine sidechain, ethylmethylsulfide for methionine and toluene for phenylalanine (see Figure 1). For this preliminary study the binding constant was determined for each fragment using the HFE parameter set of Merz with the following procedure:

1. We performed MD based Umbrella Sampling (US) simulations in explicit water to sample along the reaction coordinate of binding, i.e. the distance between silver(I) ion and the coordinated atom;[14]
2. The Potential of Mean Force (PMF) was determined along the binding reaction coordinate through WHAM;[15]
3. From the PMF, the binding constant $\log_{10}(K_{bind,calc})$ was calculated (and, consequently, the binding free energy $\Delta G_{bind,calc}$).[16]

We then compared the calculated binding constant with the experimental one from NIST database or from measured values by spectrophotometric titrations (see ESI),[17] and performed a calibration if necessary.

As a side note, our initial test calculations for HEFM were carried out with CHARMM's modified TIP3P (cTIP3P) model in contrast to the parametrizations of Merz or Won that were carried out with Jorgensen's original TIP3P model (sTIP3P). To probe the influence of the two TIP3P solvation models we calculated the PMFs and binding constants of the fragments for both water models.

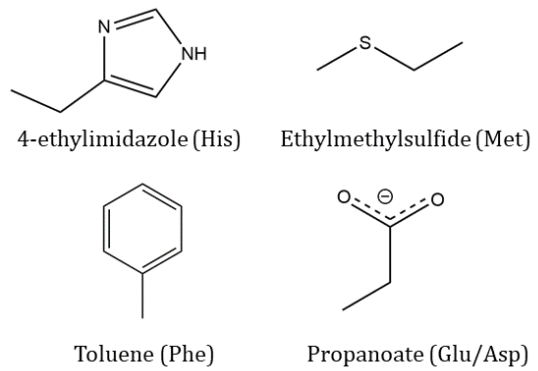

Figure 1: Sidechain fragments to represent histidine, methionine, phenylalanine and glutamic/aspartic acid.

2.2 Calibration of NBFIX parameters

Correction terms for the 12-6 LJ model were developed to better model the silver(I)-methionine and silver(I)-histidine interactions in particular. The modeling of histidine sidechain is a special case. Indeed, depending on pH, four tautomeric forms are theoretically possible (see Figure 2): one positively charged with both N atoms of the imidazole ring protonated (HSP in CHARMM or HIP in AMBER), two neutral forms with either the proton on the N-δ (HSD or HID) or on the N-ε (HSE or HIE), and one negatively charged form with no protons on the N atoms (that is, imidazolate-like form). The latter is very rare in biological contexts (see PDB entry 7WAA for an example) as it requires very basic conditions (pK_a =12-14).[18,19] The HSE tautomer was observed by NMR experiments and in many crystal structures of silver(I)-binding small peptides.[9,20] In addition, quantum mechanical calculations showed that 4-ethylimidazole (HSE tautomer) features a higher binding constant than 5-ethylimidazole (HSD tautomer).[21] For these reasons, in this work we only considered the HSE tautomer (and thus 4-ethylimidazole as sidechain representative molecule), where silver(I) can bind only to the nitrogen N-δ. Under certain conditions, however, the silver(I) ion can bind to the N-ε nitrogen, for example in the SilF, where the histidine is buried inside the protein and the HSD tautomer is stabilized through specific interactions. The possibility to include the biologically relevant tautomers through constant-pH computer simulations is discussed in the conclusion.

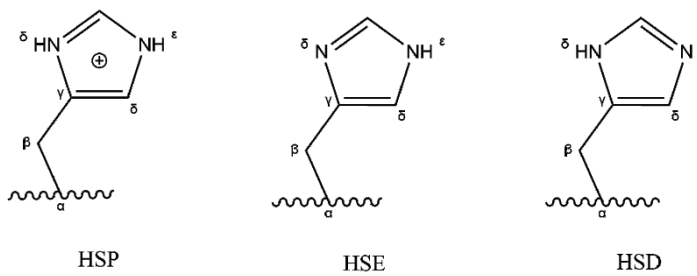

Figure 2: Tautomers of the histidine sidechains as defined in CHARMM force field family: HSP (left, positive), HSE (center, neutral) and HSD (right, neutral).

To determine correction terms for the nonbonded interaction of silver(I), we exploited the NBFIX feature of the CHARMM family of force fields, which easily allows one to specify the atoms pair parameters, ε and R^{min}, for a particular atom type-atom type interaction to adjust the LJ term of the force field without affecting the other interactions. The atoms pair parameters ε and R^{min} are derived from the Lorentz-Berthelot rules combining the parameters of the *i*-th and *j*-th atom:

$$R^{min} = \frac{R_i^{min}}{2} + \frac{R_j^{min}}{2}$$
$$\varepsilon = \sqrt{\varepsilon_i \varepsilon_j}$$

which yields the following nonbonded potential for pairwise interactions:

$$E_{NB} = E_{elec} + E_{LJ} = \frac{q_i q_j}{4\pi\varepsilon_0} + \varepsilon\left[\left(\frac{R^{min}}{r}\right)^{12} - 2\left(\frac{R^{min}}{r}\right)^{6}\right]$$

where r is the distance between the two atoms i and j, q_i and q_j are their partial charges, and ε_0 is the permittivity of vacuum. We here focus on the E_{LJ} potential, without changing the E_{elec} potential.

As a starting point for our optimization we selected the 12-6 LJ HFE parameter set. A calibration procedure was performed to determine the NBFIX pair of R^{min}, ε (referred to as only NBFIX parameters from now on) that is able to correctly reproduce the experimental binding constant of sidechain fragments. The procedure was the following:

1. Target equilibrium distances ($d_{eq,target}$, Table 2) between silver(I) and coordinated atoms of each fragment were taken either from the literature or determined by DFT calculations; target binding constants ($\log_{10}(K_{bind,exp})$, Table 2) correspond to those of the experiments (see above);
2. Using the procedure given in the section 2.1, the PMF and binding constant are calculated;
3. If the minimum of the PMF matches the target distance, we move to the next step; otherwise R^{min} is adjusted and step 2 is repeated;
4. If the calculated binding free energy is within a given error threshold of 0.5 kcal/mol, the NBFIX parameters are accepted, otherwise ε is adjusted and steps 2-3 are repeated.

2.3 Validation on HXXM and MXXH silver-binding motifs and LP1 oligopeptide

The goal of this step was to check the efficacy of the NBFIX parameters when transferred to a larger system. The validation involved calculating two different properties:

1. The binding constant of four silver-binding tetrapeptides: HEFM, MNEH, HAAM and MAAH;
2. The α-helical content in a longer peptide, LP1 (sequence: AHQKMVESHQRMMG), which was observed to form an α-helical structure upon addition of silver(I) ions.[9]

In both cases, potential-scaled molecular dynamics was employed by scaling down ε to speed up the kinetics of the dissociation process (and adjusting R^{min} so as to have the same equilibrium distance). Hamiltonian Reweighting was then used to retrieve the unbiased binding constant (ESI).

To evaluate the ability of silver(I) to favor the formation of α-helix in LP1, two simulations were performed in parallel. In one the LP1 peptide was simulated alone in solution, whereas in the other it was simulated in the presence of one silver(I) ion. After that, the α-helical content was monitored (see ESI) and compared for the two cases.

3 Results & Discussion

3.1 Testing the state-of-the-art parameters on HEFM tetrapeptide

The binding constants obtained prior the calibration procedure on the HEFM peptide are reported in Table 1 ($\log_{10}K_{bind,exp}$=6.6).[6] The values are reported for different cases, combining box size (30 and 50 Å, to verify potential size

Table 1: Initial MD simulations results for HEFM peptide. Three blocks of simulations of 100 ns each were performed for two box sizes and for each parameter set. Values are given with standard error of the mean from block analysis.

Box side (nm)	Parameters	$Log_{10}(K_{bind,calc})$
3	Won	0.8 ± 0.1
	HFE	1.0 ± 0.1
	IOD	0.5 ±0.1
5	HFE	0.8 ± 0.2
	IOD	0.6 ± 0.1

effects) and parameters set (Won, HFE and IOD). In all cases we can notice that the binding constants are lower or equal to 10, meaning a substantial underestimation of the interaction between silver(I) and the HEFM peptide is present. Since these parameters were initially not developed for reproducing peptide affinities these results are not surprising.

3.2 Calibration on sidechain fragments

The NBFIX parameters optimized to reproduce the experimental binding constant of the sidechains fragments are reported in Table 2, together with the calculated and experimental binding constants. The fragments 4-ethylimidazole and ethylmethylsulfide possess the highest experimental binding constants of 3.85 and 3.6 respectively, in logarithmic scale.

This can explain the high binding constants of the peptides containing such residues ($\log(K_{bind,exp})$=5-6.7).

In the CHARMM36m force field the sulfur of methionine is basically charge neutral (-0.08 *e*) which means that there is no electrostatic stabilization for the interaction with silver(I). Thus, a very strong NBFIX correction (high ε in absolute terms) needs to be applied on the sulfur atom of ethylmethylsulfide in order to correct its affinity. This result can be better appreciated observing Figure 3, which contains the PMF profiles of the four sidechain fragments of the peptide HEFM before (i.e. HFE parameter set) and after the calibration (in black and red lines, respectively) for both CHARMM-modified and standard TIP3P water models (cTIP3P and sTIP3P, respectively). Each line is plotted together with the standard error of the mean over the four blocks of simulation (lighter colors; merely visible due to their small magnitude). As a general observation, the HFE set *per se* drastically underestimates the affinity of silver(I) for 4-ethylimidazole and ethylmethylsulfide. There should be no surprise in this, because those parameters were developed to model silver(I)-water interaction only, without any intended correction for

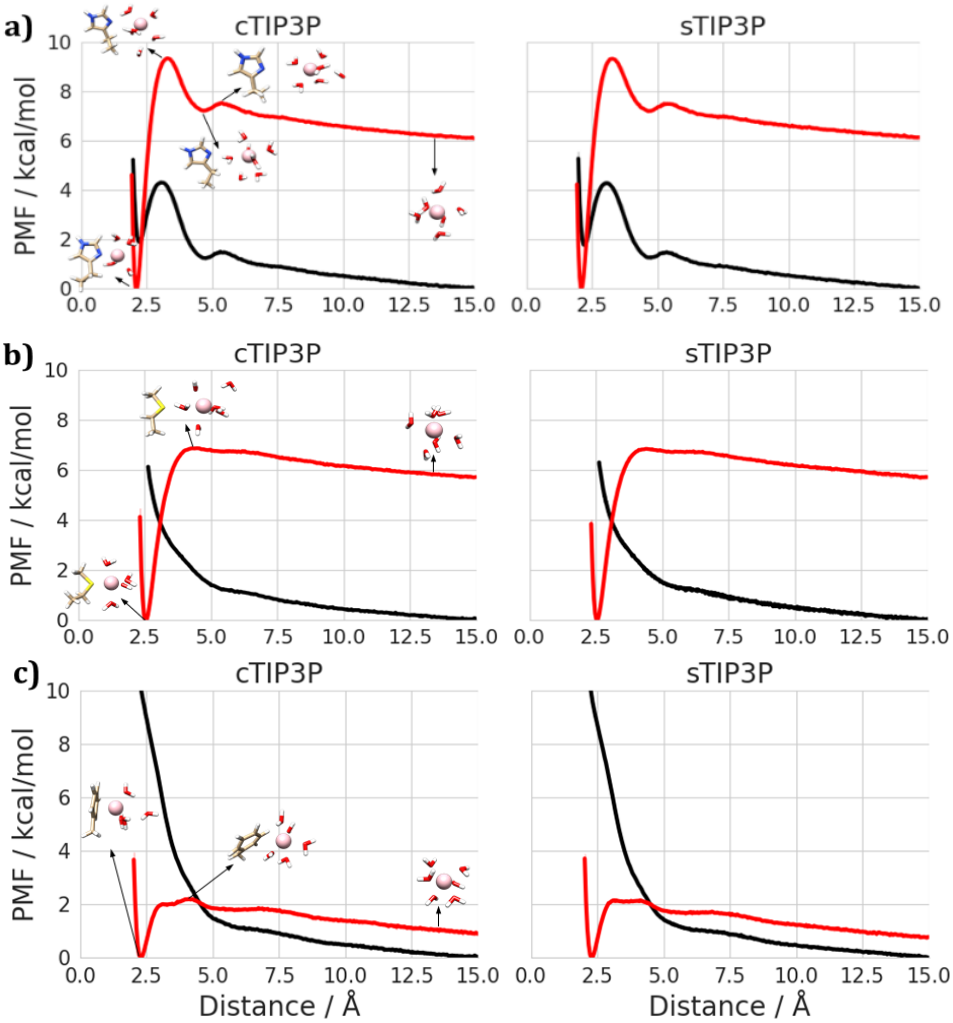

Figure 3: PMF profiles and structures of (a) 4-ethylimidazole, (b) ethylmethylsulfide and (c) toluene with HFE only parameters (black line) and with NBFIX parameters (red line) and in cTIP3P (left) and sTIP3P (right) water models. Lines are plotted together with the standard error of the mean (lighter colors). For propanoate, the distance refers to the one from the carboxylic C atom. For toluene, the distance refers to the one from the center of the aromatic ring. Structures are reported for the cTIP3P water model.

Table 2: Optimized NBFIX ε (kcal/mol) and R^{min} (Å) parameters after the calibration for the sidechains representative molecules. Results are reported for the two water models cTIP3P and sTIP3P. Calculated association constants are reported together with the standard error of the mean from block analysis. Calculated and experimental target equilibrium distances $d_{eq,calc}$ (corresponding to the minimum of the PMF profile) and $d_{eq,target}$ are also reported.

Sidechain fragment	Water model	ε	R^{min}	$d_{eq,calc}$ [a]	$d_{eq,target}$ [b]	$\log_{10}(K_{bind,calc})$ (HFE)	$\log_{10}(K_{bind,calc})$ (with NBFIX)	$\log_{10}(K_{bind,exp})$
4-ethylimidazole	cTIP3P	-4.7	2.25	2.08	2.05-2.2[c]	-1.50 ± 0.02	3.82 ± 0.02	3.85[d]
	sTIP3P	-4.4	2.25	2.11		-0.15 ± 0.01	3.86 ± 0.03	
Ethylmethylsulfide	cTIP3P	-11.9	2.50	2.55	2.3-2.5[e]	-1.89 ± 0.02	3.70 ± 0.02	3.6[d] -3.7[f,g]
	sTIP3P	-11.85	2.50	2.54		-0.29 ± 0.01	3.71 ± 0.03	
Toluene	cTIP3P	-1.77	2.65	2.29[h]	2.3[i]	-2.43 ± 0.03	0.43 ± 0.06	0.44[g]
	sTIP3P	-1.715	2.65	2.29[h]		-2.42 ± 0.01	0.43± 0.03	
Propanoate	cTIP3P	None	None	2.43[j]	2.1-2.4[k]	0.89 ± 0.03	0.89 ± 0.03	0.73[g,l]
	sTIP3P	None	None	2.43[j]		1.25 ± 0.02	1.25 ± 0.02	

[a] From the minimum of the PMF profile.
[b] Experimental target equilibrium distance (see text).
[c] Refs. 20, 22.
[d] From this work (SI).
[e] Refs. 22, 23.
[f] Measured for dimethylsulfide.[24]
[g] NIST database. [17]
[h] Referred to the distance from the center of the aromatic ring.
[i] From DFT calculations.
[j] Referred to the distance from the carboxyl C atom.
[k] Ref. 25.
[l] Measured for acetic acid.

interactions with solutes. In particular, in the case of ethylmethylsulfide and toluene, the interaction passes from repulsive to attractive after the calibration procedure, which explains why the binding constant of the HEFM peptide was drastically underestimated during the preliminary evaluations. In the case of propanoate, no NBFIX correction was needed, as the calculated binding constants were reasonably close to the experimental value (0.89 and 1.25 versus 0.73, respectively for cTIP3P and sTIP3P, see ESI for the PMF profile) as well as the equilibrium distance.

Table 3: Calculated binding constants for the studied tetrapeptides (HEFM, MNEH, HAAM and MAAH). The results are shown for both cTIP3P and sTIP3P. Calculated association constants are reported together with the standard error of the mean from block analysis.

Peptide	Water model	$\log_{10}(K_{bind,calc})$	$\log_{10}(K_{bind,exp})$
HEFM	cTIP3P	6.0 ± 0.1	6.6 ± 0.1
	sTIP3P	6.0 ± 0.2	
MNEH	cTIP3P	5.8 ± 0.1	5.4 ± 0.1
	sTIP3P	5.8 ± 0.1	
HAAM	cTIP3P	5.9 ± 0.1	5.7 ± 0.1
	sTIP3P	6.1 ± 0.1	
MAAH	cTIP3P	5.9 ± 0.1	5.3 ± 0.1
	sTIP3P	5.9 ± 0.1	

3.3 Validation on four silver-binding tetrapeptides

Table 3 reports the calculated binding constants adopting the NBFIX parameters sets for the four silver-binding tetrapeptides HEFM, MNEH, HAAM and MAAH. Overall, the calculated binding constants are on the same order of magnitude as the experimental values. In terms of Gibb's free energy, they are within 1 kcal/mol from the experimental reference values. Moreover, no significant difference is found when comparing cTIP3P and sTIP3P. Whereas the experiment predicts subtle differences between these peptides in terms of affinity, the calculations predict basically the same value for all peptides. A potential reason for this levelling/flattening is the neglection of the histidine tautomerism in the calculations above.

Here we would like to remind the reader that the HSE tautomer is the preferred silver(I)-binding tautomer for small peptides (see above).

According to constant-pH simulation of the apo form, the MAAH peptide displays a significantly decreased population of the preferred HSE tautomer (36%) with respect to HAAM (60%) (see ESI of the cited article).[7] Thus, there is a larger tautomeric penalty to overcome for MAAH than for HAAM. As a result, the calculated binding constant with tautomeric correction $\log(K_{ass,corr})$ is 0.22 lower for MAAH (5.47) than for HAAM (5.69) in excellent agreement with the experiment (5.4 ± 0.1 and 5.7 ± 0.1 for MAAH and HAAM, respectively).

3.4 Application to LP1

As a further validation of the parameters, the ability to reproduce structural features such as the α-helical content of the longer silver-binding peptide LP1 was tested. Figure 4 reports the percentage of average α-helical content in the LP1 peptide. Indeed, the presence of the silver(I) ion increases the

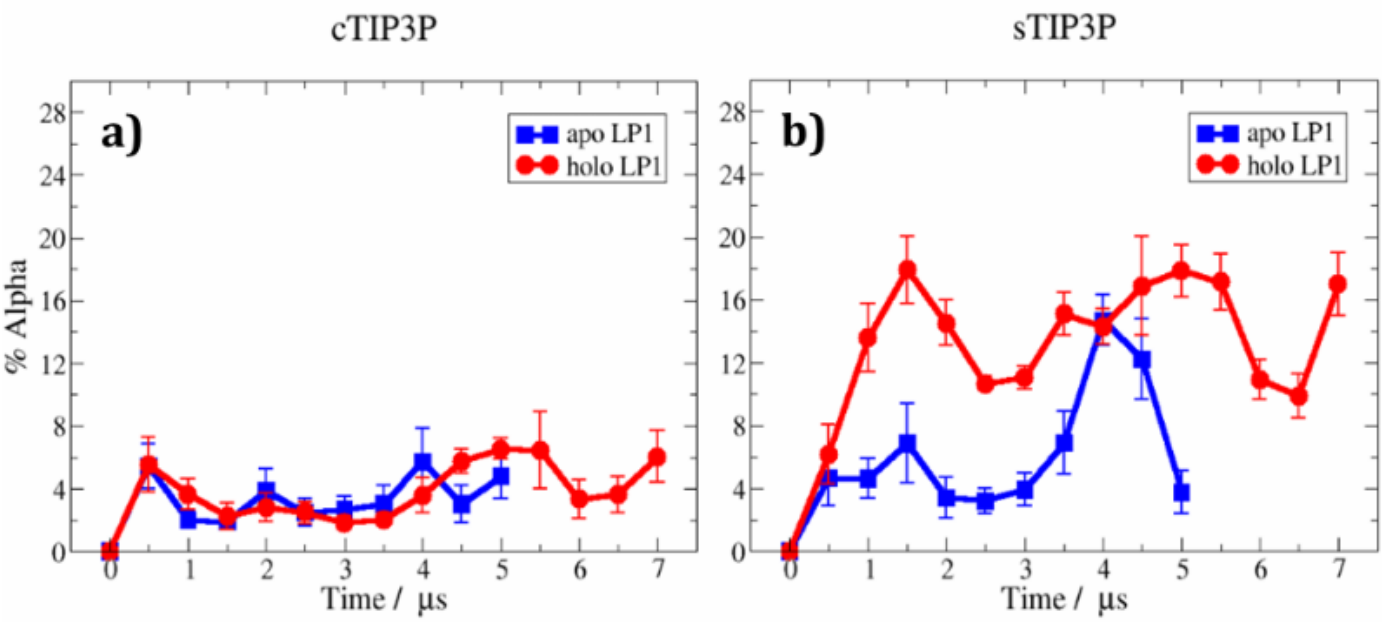

Figure 4: Percentage of α-helical content of LP1 over time (µs) for simulations in cTIP3P (a) and in sTIP3P (b) in the absence (apo, blue) and presence (holo, red) of silver(I).

α-helical content to about 17-18% in the case of the sTIP3P water model (Figure 4b). By contrast, in absence of the ion the α-helical content remains around 5-6%. It should be noted that folding of the peptide into a helix is a slow process and our simulation time of 7 µs could not capture the full dynamics. A part of the problem is that the chosen simulation approach with a scaled potential slows down the folding dynamics since the scaling favors the silver(I) dissociation from the peptide.

Furthermore, the simulations were carried out only with a single silver(I) ion in the simulation box to simplify the Hamiltonian reweighting scheme. NMR studies indicated, however, that multiple silver(I) ions can bind to LP1. Simulations with more ions are planned.

For the cTIP3P water model no induction of α-helical content can be observed.

4 Conclusion & Outlook

Our new force field parameters for silver(I) ions are capable to reproduce binding constants for tetrapeptides on the same order of magnitude as experimental values. Also, the increased α-helical content of LP1 in the presence of silver(I) was correctly detected with these new parameters. These results validate the applicability of the simple yet accurate LJ model, which can be tightly tuned by means of the NBFIX feature of the CHARMM force field family to selectively correct atom-atom nonbonded interactions, without affecting the rest of the forcefield. We anticipate that the methodology proposed in this work can be in principle applied to any metal ion provided the existence of reference data for binding constants and distances.

We note, however, further improvements for the future simulations of silver(I) interactions with peptides and proteins:

1) Histidine tautomerism. The explicit inclusion of the various protonation states of histidine (and in general on all titrable amino acids, especially for cysteine). In this work we assumed that a single static protonation state (HSE) with a microscopic binding constant that coincides with the experimental macroscopic binding constant of 4-ethylimidazole. A more realistic description would allow a dynamic change of histidine protonation states by constant pH-simulations where each state binds silver(I) with a specific microscopic binding constants.[26]

2) Polarization. This effect is particularly pertinent to deal with the coordination of two or more amino acids to the same silver(I) center as it is observed in more complex systems such as silver-binding oligopeptides (LP1) or proteins (SilE). The NBFIX LJ potentials are fully additive and therefore may lead to an overestimation of the affinity. Inclusion of polarization could be done in the context of a polarizable force field such as AMOEBA or CHARRM's Drude force field.[27,28]

3) Cationic Dummy Metal Ion Model. To account for particular coordination geometries, the extension to a model with cationic dummy charges could be beneficial.[29]

4) Extension of the parametrization to other sidechain fragments and the peptide backbone. The availability of experimental data is the limited factor here. In this light, we would like to emphasize that a careful determination of the reference parameters (equilibrium distance and binding constant) is crucial for the parametrization procedure and can highly influence the sampling.

5) Finally, improvements may result through the use of enhanced sampling techniques such as Replica Exchange.[30] This could be crucial for an integrative approach that combines the affinity simulation of silver(I) with the constant-pH feature.

Acknowledgements

The authors would like to acknowledge the High Performance Computing Center of the University of Strasbourg for supporting this work by providing scientific support and access to computing resources through grants g2023a142c/g

and g2024a236c/g. Part of the computing resources were funded by the Equipex Equip@Meso project (Programme Investissements d'Avenir) and the CPER Alsacalcul/Big Data.

The work was further supported by a grant from the Swiss National Science Foundation (Project N° 204215).

LM is grateful to the University of the Upper Alsace for a PhD stipend.

Electronic Supporting Information

Electronic Supporting Information (ESI) is available online on https://www.biorxiv.org. It contains experimental methods and computational details.

References

(1) Eckhardt, S.; Brunetto, P. S.; Gagnon, J.; Priebe, M.; Giese, B.; Fromm, K. M. Nanobio Silver: Its Interactions with Peptides and Bacteria, and Its Uses in Medicine. *Chem. Rev.* **2013**, *113* (7), 4708–4754.

(2) Silver, S.; Phung, L. T.; Silver, G. Silver as Biocides in Burn and Wound Dressings and Bacterial Resistance to Silver Compounds. *J. Ind. Microbiol. Biotechnol.* **2006**, *33* (7), 627–634.

(3) Feng, Q. L.; Wu, J.; Chen, G. Q.; Cui, F. Z.; Kim, T. N.; Kim, J. O. A Mechanistic Study of the Antibacterial Effect of Silver Ions on Escherichia Coli and Staphylococcus Aureus. *J. Biomed. Mater. Res.* **2000**, *52* (4), 662–668.

(4) Jung, W. K.; Koo, H. C.; Kim, K. W.; Shin, S.; Kim, S. H.; Park, Y. H. Antibacterial Activity and Mechanism of Action of the Silver Ion in Staphylococcus Aureus and Escherichia Coli. *Appl. Environ. Microbiol.* **2008**, *74* (7), 2171–2178.

(5) Becker, R. O. Silver Ions in the Treatment of Local Infections. *Met.-Based Drugs* **1999**, *6* (4–5), 281526.

(6) Chabert, V.; Hologne, M.; Sénèque, O.; Crochet, A.; Walker, O.; Fromm, K. M. Model Peptide Studies of Ag+ Binding Sites from the Silver Resistance Protein SilE. *Chem. Comm.* **2017**, *53* (45), 6105–6108.

(7) Bianchi, A.; Marquenet, F.; Manciocchi, L.; Spichty, M.; Fromm, K. M. Submitted to *Chem. Comm.*

(8) Silver, S. Bacterial Silver Resistance: Molecular Biology and Uses and Misuses of Silver Compounds. *FEMS Microbiol. Rev.* **2003**, *27* (2–3), 341–353.

(9) Chabert, V.; Hologne, M.; Sénèque, O.; Walker, O.; Fromm, K. M. Alpha-Helical Folding of SilE Models upon Ag(His)(Met) Motif Formation. *Chem. Comm.* **2018**, *54* (74), 10419–10422.

(10) Li, P.; Song, L. F.; Merz, K. M., Jr. Systematic Parameterization of Monovalent Ions Employing the Nonbonded Model. *J. Chem. Theory Comput.* **2015**, *11* (4), 1645–1657.

(11) Li, Z.; Song, L. F.; Sharma, G.; Koca Fındık, B.; Merz, K. M. Jr. Accurate Metal–Imidazole Interactions. *J. Chem. Theory Comput.* **2023**, *19* (2), 619–625.

(12) Jafari, M.; Li, Z.; Song, L. F.; Sagresti, L.; Brancato, G.; Merz, K. M. Jr. Thermodynamics of Metal–Acetate Interactions. *J. Phys. Chem. B* **2024**, *128* (3), 684–697.

(13) Tolbatov, I.; Marrone, A. Computational Strategies to Model the Interaction and the Reactivity of Biologically-Relevant Transition Metal Complexes. *Inorganica Chim. Acta* **2022**, *530*, 120686.

(14) Torrie, G. M.; Valleau, J. P. Nonphysical Sampling Distributions in Monte Carlo Free-Energy Estimation: Umbrella Sampling. *J. Comput. Phys.* **1977**, *23* (2), 187–199.

(15) Kumar, S.; Rosenberg, J. M.; Bouzida, D.; Swendsen, R. H.; Kollman, P. A. THE Weighted Histogram Analysis Method for Free-Energy Calculations on Biomolecules. I. The Method. *J. Comput. Chem.* **1992**, *13* (8), 1011–1021.

(16) Woo, H.-J.; Roux, B. Calculation of Absolute Protein-Ligand Binding Free Energy from Computer Simulations. *Proc. Natl. Acad. Sci. U.S.A.* **2005**, *102* (19), 6825–6830.

(17) Burgess, D. R. NIST Critically Selected Stability Constants of Metal Complexes: Version 8.0. 2004.

(18) Sjöberg, S. Critical Evaluation of Stability Constants of Metal-Imidazole and Metal-Histamine Systems (Technical Report). *Pure Appl. Chem.* **1997**, *69* (7), 1549–1570.

(19) Zhang, Q.; Wang, R.; Wang, M.; Liu, C.; Koohi-Moghadam, M.; Wang, H.; Ho, P.-L.; Li, H.; Sun, H. Re-Sensitization of Mcr Carrying Multidrug Resistant Bacteria to Colistin by Silver. *Proc. Natl. Acad. Sci. U.S.A.* **2022**, *119* (11), e2119417119.

(20) Nomiya, K.; Takahashi, S.; Noguchi, R.; Nemoto, S.; Takayama, T.; Oda, M. Synthesis and Characterization of Water-Soluble Silver(I) Complexes with l-Histidine (H2his) and (S)-(−)-2-Pyrrolidone-5-Carboxylic Acid (H2pyrrld) Showing a Wide Spectrum of Effective Antibacterial and Antifungal Activities. Crystal Structures of Chiral Helical Polymers [Ag(Hhis)]n and {[Ag(Hpyrrld)]2}n in the Solid State. *Inorg. Chem.* **2000**, *39* (15), 3301–3311.

(21) Manciocchi, L.; Spichty, M. Journal in Preparation.

(22) Modder, J. F.; Vrieze, K.; Spek, A. L.; Challa, G.; Van Koten, G. Stereoregular Coordination Polymers Formed on Binding of Peptide-Based Polydentate Ligands to Silver(I) and Copper(I). X-Ray Structure of ([Ag{N-[N-((5-Methyl-2-Thienyl)Methylidene)-L-Methionyl]Histamine}]+[O3SCF3]-.MeOH).Infin. and a Solution Structure Study. *Inorg. Chem.* **1992**, *31* (7), 1238–1247.

(23) Kasuga, N. C.; Yoshikawa, R.; Sakai, Y.; Nomiya, K. Syntheses, Structures, and Antimicrobial Activities of Remarkably Light-Stable and Water-Soluble Silver Complexes with Amino Acid Derivatives, Silver(I) *N* -Acetylmethioninates. *Inorg. Chem.* **2012**, *51* (3), 1640–1647.

(24) Sigel, H.; Scheller, K. H.; Rheinberger, V. M.; Fischer, B. E. Comparison of the Ligating Properties of Disulphides and Thioethers: Dimethyl Disulphide, Dimethyl Sulphide, and Related Ligands. *J. Chem. Soc. Dalton Trans.* **1980**, *7*, 1022–1028.

(25) Olson, L. P.; Whitcomb, D. R.; Rajeswaran, M.; Blanton, T. N.; Stwertka, B. J. The Simple Yet Elusive Crystal Structure of Silver Acetate and the Role of the Ag–Ag Bond in the Formation

of Silver Nanoparticles during the Thermally Induced Reduction of Silver Carboxylates. *Chem. Mater.* **2006**, *18* (6), 1667–1674.

(26) Aho, N.; Buslaev, P.; Jansen, A.; Bauer, P.; Groenhof, G.; Hess, B. Scalable Constant PH Molecular Dynamics in GROMACS. *J. Chem. Theory Comput.* **2022**, *18* (10), 6148–6160.

(27) Ren, P.; Ponder, J. W. Polarizable Atomic Multipole Water Model for Molecular Mechanics Simulation. *J. Phys. Chem. B* **2003**, *107* (24), 5933–5947.

(28) Anisimov, V. M.; Lamoureux, G.; Vorobyov, I. V.; Huang, N.; Roux, B.; MacKerell, A. D. Determination of Electrostatic Parameters for a Polarizable Force Field Based on the Classical Drude Oscillator. *J. Chem. Theory Comput.* **2005**, *1* (1), 153–168.

(29) Duarte, F.; Bauer, P.; Barrozo, A.; Amrein, B. A.; Purg, M.; Åqvist, J.; Kamerlin, S. C. L. Force Field Independent Metal Parameters Using a Nonbonded Dummy Model. *J. Phys. Chem. B* **2014**, *118* (16), 4351–4362.

(30) Qi, R.; Wei, G.; Ma, B.; Nussinov, R. Replica Exchange Molecular Dynamics: A Practical Application Protocol with Solutions to Common Problems and a Peptide Aggregation and Self-Assembly Example. *Methods Mol. Biol. Clifton NJ* **2018**, *1777*, 101–119.